2006

Hurricane Isabel (2003): new insights into the physics of intense storms Pt.1 mean vortex structure and maximum intensity estimates

Hurricane Isabel (2003): New Insights into the Physics of Intense Storms

Part I - Mean Vortex Structure and Maximum Intensity Estimates

Michael T. Montgomery*

Department of Atmospheric Science

Colorado State University

Fort Collins, CO

Michael M. Bell

Colorado State University/NCAR

Fort Collins/Boulder CO

Sim D. Aberson

NOAA/AOML/Hurricane Research Division

Miami, FL

Michael L. Black

NOAA/AOML/Hurricane Research Division

Miami, FL

Submitted: Bulletin of the American Meteorological Society, 19 May 2005

Revised: 18 May, 2006.

*Present affiliation: Department of Meteorology, Naval Postgraduate School, Monterey, CA &

NOAA's Hurricane Research Division, Miami, FL.

From a science point of view, I love how the atmosphere likes to throw curve balls when people think they understand `everything.'

--*Lance Bosart*

Abstract

This study is an observational analysis of the inner-core structure, sea surface temperature, outflow layer, and atmospheric boundary layer of an intense tropical cyclone whose intensity and structure is consistent with recent numerical and theoretical predictions of *superintense* storms. The findings suggest new scientific challenges for the current understanding of hurricanes.

Unprecedented observations of category 5 Hurricane Isabel (2003) were collected during 12 – 14 September. This two-part series reports novel dynamic and thermodynamic aspects of the inner-core structure of Isabel on 13 September made possible by analysis of these data. Here, a composite of the axisymmetric structure of the inner-core and environment of Isabel is estimated using Geostationary Positioning System dropwindsondes and in-situ aircraft data. In Part II, an extreme wind speed observation on the same day is discussed in the context of this work.

The axisymmetric data composite suggests a reservoir of high entropy air inside the low-level eye and significant penetration of inflowing near-surface air from outside. The analysis suggests that the low-level air penetrating the eye is enhanced thermodynamically by acquiring additional entropy through interaction with the ocean and replaces air mixed out of the eye. The results support the hypothesis that this high entropy eye air "turbo-boosts" the hurricane engine upon its injection into the eyewall clouds. Recent estimates of the ratio of sea-to-air enthalpy and momentum exchange at high wind speed are used to suggest that Isabel utilized this extra power to exceed the previously assumed intensity upper bound by 10 to 35 m s^{-1} for the given

environmental conditions. Additional study with other data sets is encouraged to further test the superintensity hypothesis.

1. Introduction

Hurricane Isabel was at or near category 5 on the Saffir-Simpson scale (surface wind speed > 67 m s^{-1}) from 12 – 14 September 2003. On 13 September, the strongest known horizontal wind (107 ms^{-1}) recorded in a hurricane was obtained by a NCAR GPS dropwindsonde at 1752 UTC (Aberson et al. 2005; Hock and Franklin 1999)[1]. Multiple aircraft missions by NOAA and U. S. Air Force Hurricane Hunters obtained a uniquely comprehensive observational dataset during this period. Multiple dropwindsondes, in-situ flight level data, airborne Doppler radar data, and high-resolution satellite imagery provide an unprecedented view of the kinematic and thermodynamic structure of Isabel over three days. A synthesis of flight-level and dropwindsonde data during 12 - 14 September along with a detailed description of the dataset and analysis methodology is reported elsewhere (Bell and Montgomery 2006); the focus of this two-part study is the analysis for 13 September.

A nearly circular core of deep eyewall convection at 2218 UTC on 13 September is represented in Fig. 1a by the cold (red) 85 GHz brightness temperature. Non-axisymmetric structures inside the eye with cloud bands connecting to the eyewall are also apparent in the low-level stratus clouds at 1745 UTC (Fig. 1b), along with a pentagon-shaped region of high reflectivity seen in a NOAA P-3 lower fuselage radar image at approximately the same time (Fig. 1c). These observations, in conjunction with GOES super-rapid-scan animations (not shown), corroborate the existence of coherent mesovortices in the vicinity of the eyewall that have been predicted by high resolution numerical simulations (Schubert et al. 1999, hereafter S99; Kossin and Schubert 2001; Persing and Montgomery 2003, hereafter PM03; Kossin and Schubert 2004)

[1]A report of 117 ms^{-1} from a dropwindsonde released in Hurricane Katrina (2005) is unconfirmed due to apparent loss of the raw data.

and liquid-water laboratory experiments (Montgomery et al. 2002 and refs.). The mesovortices are believed to be the result of a combined barotropic/baroclinic instability associated with an annulus of high potential vorticity near and within the eyewall cloud that is generated by latent heating and vortex tube stretching (S99; Nolan and Montgomery 2002).

In addition to contributing to localized extreme winds, evidence suggests that eyewall mesovortices in the lower troposphere can actually enhance the storm-scale energetics. In simple models that neglect diabatic processes and/or the secondary circulation, eyewall wave and vortex structures exert a cyclonic torque on the eye, thereby spinning up the eye at the expense of the maximum tangential winds (Rotunno 1978; Smith 1980; Emanuel 1997; S99, Kossin and Schubert 2001). However, in conjunction with a secondary circulation driven by latent heating, surface friction and eddy processes, the breakdown of the eyewall and the corresponding (vorticity) mixing associated with the enstrophy cascade permits low-level inflowing air parcels to penetrate the highly impermeable eyewall (Rotunno 1984, S99). Parcels that reach the low-level eye and spend sufficient time inside it can increase their moist entropy above eyewall values through interaction with the ocean and because of the reduced surface pressure relative to that in the eyewall. From an energetics viewpoint, then, the net effect of the mean secondary and eddy circulation within the low-level eye is to transport and stir high-entropy air from the eye to the eyewall (S99; Braun 2002; PM03; Braun et al. 2005; Cram et al. 2006; Eastin et al. 2005). In this way, the low-level eye can provide additional power to the hurricane engine relative to that obtained from the ocean underneath the eyewall where current theory assumes all the heat uptake occurs (cf. Emanuel 1997).

For the first time, observations suggest that this thermodynamic boost exceeds the weakening tendency associated with the breakdown of the eyewall. By utilizing this additional power, the hurricane can, in principle, obtain a “superintense” state with azimuthally-averaged

tangential winds faster than previously-predicted upper bounds for the mean tangential wind at the swirling boundary layer top, as predicted by Emanuel and colleagues (Emanuel 1986, hereafter E86; Rotunno and Emanuel 1987, hereafter RE87; Emanuel 1988, 1991, 1995, 1997, hereafter E88, E91, E95 & E97, respectively; Bister and Emanuel 1998, hereafter BE98; Emanuel et al. 2004, hereafter E04). This theoretical upper bound, or maximum potential intensity (MPI), for given environmental conditions is referred to hereafter as E-MPI. The current work is believed to be the first study using sufficiently detailed *in-situ* observations to test E-MPI theory and to suggest the existence of superintense storms in nature previously predicted using high-resolution computer simulations (PM03).

A detailed analysis of the dropwindsonde and flight-level data as they relate to the estimated azimuthal mean structure of Isabel on 13 September is provided in Part I. A record horizontal wind speed measured on the same day is presented in Part II, along with a discussion of similar observations from other intense storms. Together, these studies suggest new insight into the thermomechanics of intense hurricanes. The observations are consistent with high resolution numerical simulations that produce superintense storms. An outline of the remaining sections of Part I follows: Section 2 provides the methodology and analysis of the estimated mean inner-core structure of Isabel. Section 3 presents an analysis of environmental conditions and *a priori* E-MPI estimates. Concluding remarks are given in Section 4.

2. Estimated mean vortex structure

a. Data overview

A two-dimensional analysis of the axisymmetric kinematic and thermodynamic structures of Isabel in the radial-vertical plane was performed using in situ flight-level data and 28 eyewall and eye dropwindsondes released from three aircraft (two NOAA P-3s and a USAF C-130) flying at different altitudes. The sweeping dropwindsonde trajectories and multiple aircraft

penetrations into the hurricane (Fig. 2a) show the uniform azimuthal data coverage obtained from 16 – 23 UTC on 13 September. The high radial and vertical resolutions of the ~30,700 data points (approximately half from the dropwindsondes) recorded during this time period are depicted in Fig. 2b. Although the dense spatial resolution allows for high confidence in retrieved axisymmetric features in the eyewall region, greater uncertainty in the axisymmetric component exists inside 30 km radius where the sampling was limited. In particular, the limited observations inside this radius preclude a meaningful separation of the kinematic and thermodynamic quantities into azimuthal mean (vortex) and asymmetric (eddy) components there. Although these innermost data are included in the composite, the estimated axisymmetric structure is likely quantitatively inaccurate there due to large-amplitude mesovortex structures evident in the GOES super-rapid-scan animations and video recordings taken aboard the NOAA P-3 while flying inside the eye of Isabel.

b. Compositing technique

The dropwindsonde and in-situ data were composited relative to a moving (~7 m s^{-1}) storm center using the Barnes objective analysis technique (Barnes 1973; Koch et al. 1983). Although temporal evolution is not resolved by this method, the data and quality control parameters suggest that Isabel was nearly steady state during the time period of the analysis. Whereas the Barnes objective analysis has been used extensively with synoptic and satellite data, its application for inferring radius-height mean hurricane structure is believed to be novel. Different grid sizes were used in the vertical (250 m) and the radial (2500 m) directions, with weighting functions allowing for resolving of features on scales of greater than 1 km and 10 km, respectively, to account for the relatively shallow observations indicated in Fig. 2. All data were treated as azimuthally independent, combining the primarily Eulerian aircraft data with the Lagrangian dropwindsonde data, by their location in the radius-height plane. Storm-relative

tangential and radial wind velocities were calculated by subtracting the storm motion at appropriate times derived from aircraft center fixes. Vertical velocity was measured at flight level by the aircraft inertial navigation system, and was also calculated along the dropwindsonde trajectory by removing the terminal fall speed from the measured dropwindsonde motion. The analyzed secondary circulation does not everywhere satisfy the continuity equation, due to uncertainty in the analysis of the axisymmetric radial wind arising from under-sampling (e.g., near 15 km radius from storm center, see Fig. 3), uncertainty in the precise location of the circulation center, and the estimated dropwindsonde terminal fall speed. Asymmetries not considered here may also contribute to the disagreement between measured vertical velocities and those calculated from mass continuity. The resulting transverse circulation components are nevertheless self-consistent and are believed to capture the zero-order features of the axisymmetric transverse circulation.

c. Derived mean structure and evidence supporting the "superintensity" mechanism

The kinematic and thermodynamic structure of Isabel derived from GPS dropwindsonde and flight-level data is displayed in the radius-height composites of storm-relative tangential and radial wind velocities (Fig. 3a) and equivalent potential temperature, specific absolute vertical angular momentum, and transverse secondary circulation vectors (Fig. 3b). The specific absolute vertical angular momentum (absolute circulation) is defined as $M=rv + {}^{1}\!/_{2} fr^2$ where r is the radius from the vortex center, v is the storm-relative tangential wind, and f is the Coriolis parameter.

The maximum azimuthally averaged tangential wind speed (76 ms^{-1}) is located approximately 42 km radius from the center near 1000 m above the surface. Because this is an azimuthal average, it is likely comparable to a sustained wind at this level. The strong tangential wind gradient along the inner edge of the eyewall is consistent with local Kelvin-Helmholtz

(shear) instabilities and associated lateral mixing across the eyewall interface implied by the satellite and radar imagery in Fig. 1b and 1c. (e.g., S99; Montgomery et al. 2002). An extreme wind speed maximum (107 ms^{-1}) that would likely have been recorded by an anemometer as a gust, was observed by a dropwindsonde near 30 km radius at 1.4 km altitude (see Part II, Aberson et al. 2006, for details). Near this radius, the tangential velocity was highly variable azimuthally, as would be expected with the presence of mesovortices in the eye-eyewall interface as seen in satellite imagery. Lowest-level (0-250 m) radial inflow of 20 ms^{-1} is located 25 km radius from the center, suggesting significant penetration of air from under the eyewall into the eye. Strong, inflowing air that breaches the eyewall is modified by sea-to-air latent heat flux inside the eye where widespread downdrafts that ordinarily tend to limit the ocean energy gain outside the eyewall do not exist (e.g., E86; Eastin et al. 2005). Despite the rapid decrease of mean tangential wind speed inside the eye, the low pressure and significant inflow and convergence near the surface support non-zero and persistent sea-to-air latent heat flux within the eye, thus maintaining a reservoir of high θ_e air that has been found in previous studies (LeeJoice 2000; Braun 2002; PM03; Eastin et al. 2005). High entropy air returns to the eyewall in the outflow above 1 km, indicated by the outward bulge in the θ_e contours there (Fig. 3b). The small outward bulge in the absolute angular momentum near 37 km radius and 2 km altitude provides additional evidence of this exchange, consistent with an injection of this high θ_e air into the eyewall.

Continuous penetration of low-level air into the eye is believed to replenish the eye reservoir. The combined mean and asymmetric eddy flux of high θ_e air from the low-level eye into the eyewall represents an additional power source to the hurricane heat engine. This "turbo-boost" of the engine invokes significant surface enthalpy fluxes well inside the radius at which E-MPI theory assumes they operate (PM03; cf. E95, E97, and BE98).

d. Low-level structure

The azimuthal mean low-level (0 < z < 2 km) kinematic and thermodynamic structures in the eye (r < 15 km), near the radius of maximum tangential wind (RMW) (40 km < r < 50 km), outer core (r ~200 km), and storm environment (300 km < r < 1000 km) are shown in Fig. 4. Mean soundings with 50 m vertical resolution were constructed within these radial rings. The mean sounding near the RMW shows a shallow θ_v mixed layer depth of only about 150 m, whereas the deep inflow layer extends up to 1.2 km. The maximum average tangential wind speed of ~76 m s^{-1} near 1000 m is above the strong inflow. Whereas tangential and radial wind speeds of 27 m s^{-1} and 11 m s^{-1}, respectively, are found in the outer core, only weak tangential wind and radial outflow exists inside the eye, and only weak inflow is present in the ambient environment. The relative humidity (RH) is greater than 90% in the lowest 2 km, indicating nearly saturated conditions even in the sub-cloud layer. The 0 - 50 m air temperature of ~24 ˚C near the RMW indicates a ~3.5 K cooling from the outer core and environment. However, the low-level eye temperature is 1.5 ˚C higher than near the RMW. The ambient average θ_e in the mixed layer (~500 m deep) increases from 350 K to 354 K in the outer core (~200 km radius), and then increases an additional 3 K as the air approaches the eyewall base at the RMW. An additional 14 K θ_e increase is available to near-surface parcels that penetrate significantly into the eye and spend some time inside it. By accessing this energy surplus and transporting it to the eyewall, the mean tangential wind may increase beyond currently formulated upper bounds. Whereas a detailed calculation of the residence time of air parcels in Isabel's eye is beyond the scope of this study, Cram et al. (2006) showed that residence times in the eye for significant θ_e gain in their numerical simulation of Hurricane Bonnie were commonly on the order of 40 – 60 minutes and as low as 15 minutes. This suggests that the eye entropy reservoir may be replenished on even relatively short time-scales.

3. Maximum Potential Intensity (MPI) Estimates

In E-MPI theory, the primary parameters needed to calculate the *a priori* MPI are: 1) the sea-surface temperature (SST) in the hurricane core; 2) upper-level exhaust (outflow) temperature where parcels undergo radiational cooling to space; 3) ambient RH near the sea surface; and (4) sea-to-air exchange coefficients of enthalpy and angular momentum. These input parameters defined in E-MPI theory (E86; RE87; E95) were calculated using available data in Hurricane Isabel and its environment. Pertinent details of these calculations are summarized here.

a. Sea Surface Temperature

The core SST (Fig. 5) was estimated from a combination of pre-storm satellite imagery, ARGOS buoy data, and low-altitude aircraft radiometer measurements. Hurricane Fabian passed through this same area ten days prior to Isabel, resulting in cooler water near the core region of Isabel than in the surrounding area during the time of the analysis. P-3 aircraft radiometer measurements (Moss 1978) from NOAA 43 recorded at ~60 and ~120 m above sea level in the wake of Isabel compare well with satellite SST estimates (McMillin and Crosby 1984; Brown and Minnett 1999; Legeckis and Zhu 1997) and suggest a 27.5 ˚C effective SST near the storm core. Given the 24˚C near-surface air temperature (Fig. 4c), a ~ 3˚C temperature deficit existed across the ocean-air interface, consistent with recent observations (Wroe and Barnes 2003; Cione et al. 2000).

For the *a priori* MPI estimates (Sec. 3d), a constant SST of 27.5 ˚C is employed to represent an effective SST during the passage of Isabel over the wake of Fabian (from 16 – 23 UTC, see Fig. 6)[2]. Although the airborne radiometer measured a reduction in SST by ~1 – 2 ˚C

[2] In E-MPI theory, the SST under the eyewall is critical for maintaining the *maximum sustained*

relative to satellite-derived SST estimates prior to Isabel's passage, this reduction is believed caused by Isabel and the corresponding shear-induced turbulent mixing from the cold thermocline (e.g., E04 and refs.). This negative feedback effect is not represented in E-MPI theory. In Sec. 3d, estimates of the impact of *storm-induced* cooling on the intensity of Isabel are presented to provide upper- and lower-bound intensity estimates.

b. Outflow temperature

Locations of soundings used to calculate the outflow temperature needed for the E-MPI calculation are shown in Fig. 6a overlaid on infrared satellite imagery indicating the minimal extent of the upper-level outflow. Without the ability to track individual air parcels through eyewall ascent and into the outflow, the outflow temperature calculation requires some modification from previous studies with numerical models (e.g., RE87). For completeness, the outflow temperature is calculated in *three ways:* (i) as a $d\ ln(\theta_e)$-weighted temperature following the original definition in E86; (ii) as an equilibrium-level temperature (the temperature at which

---

tangential wind. Here, the boundary layer air parcels spiraling inward toward the eyewall from an outer core region with an SST of ~28.5 °C are assumed to quickly lose their thermodynamic memory and to adjust rapidly to local (~27.5 °C) SST conditions on a boundary layer 'eddy-turnover' time scale $\tau \sim H/w'$, where H is the characteristic depth of the boundary layer and w' is a root-mean-square eddy vertical velocity. Letting H ~1 km and w' ~ 2 ms^{-1} gives $\tau \sim 500$ s ~ 8 min, a short time interval compared to that required for a boundary layer parcel to traverse horizontally inward from the outer-core to the eyewall (L/U~200 km /10 m s^{-1} ~ 5 h, where L represents a typical distance between the outer-core and eyewall, and U is an upper bound to the average radial inflow within this region). Alternatively, an average ambient SST of ~28.5 °C only increases the primary intensity estimate of Fig. 7 by two meters per second.

a virtual parcel starting from an ambient surface state achieves the same environmental temperature after lifting by pseudo-adiabatic ascent); and (iii) as a radial-wind-weighted temperature across the storm outflow (PM03). Table 1 presents a summary of these calculations.

The E-MPI theory (E86; RE87) uses the $d\ ln(\theta_e)$-weighted integral definition:

$$T_{out} \equiv \frac{1}{\ln\left[\frac{\theta_{ec}}{\theta_{ea}}\right]} \int_{\theta_{ea}}^{\theta_{ec}} T d\ln(\theta_e) \qquad (1)$$

where θ_{ea} and θ_{ec} denote the ambient sub-cloud layer θ_e and that of a parcel in the eyewall updraft core (r ~ 45 km, see Fig. 3b), respectively, consistent with the single-cycle Carnot model. Since θ_e is approximately conserved during ascent in the eyewall and in the upper-tropospheric outflow, $d\ ln(\theta_e)$ is approximately zero until a parcel begins its descent due to radiational cooling at large (> 300 km) radii. Assuming the θ_e profile of the sounding represents a family of parcels advected from the storm in the outflow, the integral in (1) can be performed on a single environmental sounding. The θ_e at the outflow layer bottom is assumed to be equal to θ_{ea} (E86; RE87). As an example, the outflow jet at ~ 340 km radius was sampled by a dropwindsonde (Fig. 6b) released by the NOAA Gulfstream-IV. Anticyclonic outflow extends from 11.5 km altitude up to ~14 km, with peak anticyclonic tangential wind and radial wind velocities of 13 m s^{-1} and 17 m s^{-1}, respectively. The θ_e is assumed to increase monotonically with height from 350 K to 359 K through the outflow layer. This assumption is supported by an additional measurement at ~550 km radius along the same radial (location indicated by an 'X' in Fig. 5a), where the peak outflow wind speed was ~12 m s^{-1} at 13.5 km altitude and a similar thermodynamic structure existed (not shown). In contrast, most observations of the outflow around the storm have radial wind speeds < 10 m s^{-1}, confirming that the hurricane outflow is a complex structure comprised of asymmetric outflow jets instead of the broad and homogeneous

exhaust system predicted in axisymmetric numerical models (e.g., Holland 1987; Flatau and Stevens 1989; Vladimirov et al. 2001). Note the θ_e of 354 K in the center of the outflow jet is slightly less than that observed for the sub-cloud layer at the RMW (see Fig. 4b), and approximately equal to the average θ_e across the eyewall base (cf., Houze 1993). These limits from 350 K to 359 K were used in the numerical integration of the seven environmental soundings[3] encircling the hurricane (Fig. 6a).

The temperature at the top of the boundary layer (T_B), outflow temperature (T_O), and RH from four representative environmental soundings are shown in Table 1. A range of outflow layer depths and heights are observed in four quadrants of the hurricane, with an average of the seven $d\ ln(\theta_e)$-weighted outflow temperatures of -58 ˚C (215.3 K). This value will be used as the primary system-scale outflow temperature[4]. The equilibrium-level and radial-wind-weighted outflow temperatures have been shown previously to serve as reasonable *proxies* for the $d\ ln(\theta_e)$-weighted outflow temperature and are found here to be consistent with the outflow temperature defined by (1). As an additional check, the axisymmetric thermal wind equation appropriate for a moist hurricane vortex was also used to assess the outflow temperature. This yielded consistent results and details of this calculation are summarized in the Appendix for interested readers.

---

[3] Missing data in the θ_e and wind fields were interpolated linearly between available observations in order to perform the integration. Though this smooths the radial-wind in the PM03 outflow proxy calculation, the monotonic $ln(\theta_e)$ profile is not sensitive to this.

[4] The San Juan sounding appears to be an outlier. This could be due to the high tropopause height at low latitude, the high equilibrium level since the rawinsonde was launched from land, and/or the different sensor type from the GPS dropwindsondes.

c. Relative humidity

The average RH in the lowest 500 m in these seven environmental soundings is near 80%, consistent with the boundary-layer mean structure (Fig. 4d). In the original and revised *a priori* E-MPI formulations (E86, E95), a simple closure is invoked for the near-surface RH between the environment and the region under the eyewall by assuming a constant RH between these regions. Clearly, the near-saturated conditions throughout the sub-cloud layer underneath the eyewall violate this assumption. However, E-MPI also assumes that the air parcels maintain constant temperature as they travel into the storm core. Since the observed cooling tends to offset the moistening, this yields a similar effect in the moist entropy (e.g., Camp and Montgomery 2001). For the present calculations, a simple compromise is adopted (E95; PM03) by specifying a constant 80% RH.

d. Sea-to-air exchange coefficients

For the primary intensity estimate, the ratio of bulk sea-to-air enthalpy and momentum exchange coefficients is assumed to be unity ($C_K/C_D=1$). However, observations collected during the 2002-2004 Coupled Boundary Layers Air-Sea Transfer (CBLAST) field program suggest a value of unity is an upper bound; current estimates of this ratio for a near-surface (~10 m) wind speed of approximately 50 m s^{-1} (see Fig. 4a) vary from approximately 0.5 to 0.7 (Black et al. 2006). Among the four parameters needed for the a priori MPI estimate (SST, outflow temperature, ambient RH, and C_K/C_D), the last is thought to be the most uncertain. The complex air-sea interaction processes in extreme winds are not well understood, and further research is needed to elucidate these effects more clearly (e.g., Black 2004; Sullivan et al. 2004a, b, Black et al. 2006).

e. MPI estimates: Azimuthal mean V_{max} at boundary layer top

The predicted V_{max} from the *a priori* E-MPI theory for varying outflow temperatures and near-core SSTs with a constant RH = 80% and C_K/C_D =1 are shown in Fig. 7, with the 'X' representing the primary intensity estimate. In these calculations, T_B is assumed to be ~4 ˚C lower than the SST, as suggested by the data in Table 1, and the thermodynamic efficiency is defined by

$$\varepsilon = (T_B - T_O)/ T_B. \quad (2)$$

The average efficiency for Isabel on 13 September with an SST of 27.5 ˚C is found to be 0.275. This *original* definition of the efficiency of the Carnot cycle by E86 provides a clear distinction between the SST and the air temperature at the top of the boundary layer (e.g., Houze 1993). The predictive formula used here for V_{max} is otherwise identical to a revised formulation of the Carnot model (E95) and is the basis for the values shown in Fig. 7.

A major conclusion of this study is that the observed azimuthal mean tangential wind speed at the boundary layer top (76 m s^{-1}, with a 6 m s^{-1} standard deviation) is clearly stronger than the theoretically predicted 56.6 m s^{-1} E-MPI. Warm ocean eddies do not seem to be a plausible explanation for this discrepancy given that SST observations clearly depict the cool wake left earlier by Fabian (cf. E04). Satellite data (not shown) indicate that the SST was an additional 1-2 K lower in this region *after* the passage of Isabel, suggesting that the storm-induced ocean cooling (E04) and turbulent dissipative heating (BE98) tend in opposite ways.

The (turbulent) dissipative heating effect (BE98) relative to the original *a priori* MPI (E86; E95) is calculated according to $\Delta V_{max} = V_{max}[(T_B/T_O)^{1/2}-1]$, which here represents a 9.6 ms^{-1} boost. Ocean cooling effects depend primarily on the storm translation speed and the oceanic mixed layer depth. E04 predicted a ~13 m s^{-1} intensity reduction for a storm moving at 7 m s^{-1} with a 30 m mixed layer depth (their Sec. 2c, Fig. 3). Because Isabel crossed the wake left

by Fabian (Fig. 6), Isabel likely encountered a deeper mixed layer, resulting in a somewhat reduced cooling and negative feedback effect. The estimated upper and lower bounds for the maximum intensity presented in Fig. 7 reflect uncertainties in both the bulk exchange ratio (C_K/C_D) and the storm-induced ocean cooling. The upper-bound estimate (~ 66 m s^{-1}) neglects entirely the ocean cooling caused by Isabel, includes dissipative heating, and assumes a ratio of enthalpy and momentum exchange coefficients of unity. The lower bound estimate (~40 m s^{-1}) assumes a C_K/C_D ratio of 0.5, and that the ocean cooling is compensated by the dissipative heating effect. The discrepancy between all these predicted values and the observed intensity of 76 m s^{-1} suggests a significant limitation of current E-MPI theory for this case.

4. Conclusions

For two decades, E-MPI theory often has been presented as a rigorous upper bound on hurricane intensity that is not exceeded within observational error (E86, E88, E91, E95; RE87; BE98; E04). Whereas the single-cycle Carnot model provides a good first approximation for the maximum potential intensity, the current work presents evidence that the E-MPI theory does not include a critical aspect of the inner-core structure of mature hurricanes. These in-situ observations in Hurricane Isabel suggest that the "turbo-boost" mechanism (PM03) can play an important role in providing more power to tropical cyclones and thus explain why V_{max} is substantially above this previous upper-bound for storms that lack adverse environmental influences. This V_{max} discrepancy between the *a priori* MPI theory and the observed intensity is consistent with recent high-resolution numerical model simulations, supporting the hypothesis that Isabel on 13 September was superintense as defined therein. A similar vortex-scale structure deduced from sorties flown on 12 September when the storm was even stronger (peak mean tangential wind speed at the boundary layer top > 80 m s^{-1}, not shown) suggests the turbo-boost mechanism is the most likely candidate to explain the extended period of Isabel's intense state.

More examples from this extraordinary set of observations are presented in Part II to shed insight into the exotic and complex nature of the eye-eyewall mixing phenomenon in Isabel. Whereas the observations in Part II were serendipitous, targeted observations in other intense tropical cyclones are encouraged, which, in conjunction with numerical, theoretical and laboratory work, will lead to better understanding of the heat and momentum exchange between the eye and the eyewall and to an improved maximum intensity theory.

Acknowledgments

The authors would like to acknowledge NOAA/NESDIS for their support of the Ocean Winds Experiment and NOAA and ONR (Simon Chang) for supporting the CBLAST experiment from which these data were obtained; and the pilots and support crew of the NOAA-P-3 and U.S. Air Force aircraft for their bravery and dedication to hurricane observations and science. Dropwindsondes were processed by Krystal Valde and Bill Ramstrom. We thank Pete Black, Ed Zipser, John Persing, Wen-Chau Lee, Russ Elsberry, Scott Braun, Kerry Emanuel, Tim Dunkerton, William Gray and two anonymous reviewers for constructive comments. Kerry Emanuel suggested the addition of the Appendix during the review process. This research was funded by ONR Grant N00014-02-1-0474, and NSF Grants NSF-ATM-0132006, NSF-ATM-0101781, and NSF-ATM-0349980.

Correspondence should be addressed to MTM (mike.montgomery@noaa.gov).

Appendix: Thermal Wind Balance

This appendix presents an examination of whether the deduced mean tangential wind and entropy fields presented in Fig. 3 are dynamically consistent and, given the result, a check on whether the outflow temperature computed in Sec. 3b is sufficiently cold to support the observed winds.

A thermal wind equation relating the maximum mean tangential wind speed and the radial gradient of moist entropy at the top of the boundary layer has been derived previously (E86, Eq. 13; E97, Eq. 13):

$$V_{\max}{}^2 \approx -r_m (T_B - T_O) \frac{dS_B}{dr} \qquad \text{(A1)}$$

where S_B is the moist entropy at the boundary layer top, r is the radius from the vortex center, r_m is the RMW, and other symbols are as defined in the text. Equation (A1) is a diagnostic equation that depends on the validity of the hydrostatic and axisymmetric cyclostrophic balance approximations (e.g., Holton 2004) in the eyewall of the storm. Cyclostrophic balance is a valid first approximation in the eyewall above the boundary layer where the Rossby number is large compared to unity and the flow is rotationally dominant (e.g., Willoughby 1990). The superintensity mechanism will, of course, increase the radial gradient of S_B (and thus the radial gradient of θ_e) and increase the resulting tangential wind speed. Therefore, (A1) should be valid for superintensity, as long as the winds are not appreciably supergradient. Since all quantities appearing in (A1) are calculable from the observations, the applicability of the thermal wind constraint can be assessed, and, conversely, it can be used to determine if the outflow temperature computed in Sec. 3b is sufficiently cold to support the intensity observed. Inserting the θ_e data, the radial moist entropy gradient near r ~42 km (RMW) and z =1 km (boundary layer top) is approximately:

$$\begin{aligned} \frac{dS_B}{dr} &= \frac{c_p}{\theta_e}\frac{d\theta_e}{dr} \\ &\approx \frac{1004 J/kgK}{357K} \cdot \left(\frac{-6K}{10km}\right) \\ &= -1.7\times10^{-3}\frac{m}{s^2 K}. \end{aligned} \qquad \text{(A2)}$$

Substituting this gradient into (A1), and using the values of T_B and T_O computed previously,

yields $V_{max} \approx 74$ m s^{-1}, which is close to the observed $V_{max} \approx 76$ m s^{-1} deduced from the dropwindsondes. If instead, the observed $V_{max} \approx 76$ m s^{-1} is used and the outflow temperature for the above radial entropy gradient near the RMW is inferred, one obtains $T_O \approx 216$ K, close to the outflow temperature calculated from the dropwindsonde and the Gulfstream-IV data as described in Sec. 3b.

It should be noted that this outflow temperature estimate is sensitive to the value chosen for the radial θ_e gradient. Errors from humidity sensor biases (Bell and Montgomery 2006) and spatial and temporal averaging limit the accuracy of the calculated radial entropy gradient. Deviations from axisymmetric thermal wind balance (A1) near the boundary layer top are also expected due to the mesovortices observed near the RMW. Given all of these potential errors, the consistency between the outflow temperature, the maximum tangential wind and radial entropy gradient during this analysis period is encouraging.

References

Aberson, S.D., M.T. Montgomery, M. Bell, and M. Black, 2005: Hurricane Isabel (2003): New insights into the physics of intense storms Part II: Extreme wind speeds. *Bull. Amer. Meteor. Soc.*, accepted.

Barnes, S.L., 1973: Mesoscale objective analysis using weighted time-series observations. NOAA Tech. Memo. ERL NSSL-62, National Severe Storms Laboratory, Norman, OK 73069, 60 pp.

Bell, M. M., and M. T. Montgomery, 2006: Observed structure, evolution and potential intensity of category five Hurricane Isabel (2003) from 12 – 14 September. *Mon. Wea. Rev.*, submitted.

Bister, M. and K.A. Emanuel, 1998: Dissipative heating and hurricane intensity. *Meteor. Atmos. Phys*. **65**, 233 - 240.

Black, P.G., 2004: An overview of CBLAST flights into hurricanes Fabian and Isabel (2003) *Preprints, 26th Conf. on Hurricanes and Tropical Meteorology*, Amer. Meteor. Soc., Boston MA, 1 - 2.

-----, E.A. D'Asaro, W. M. Drennan, J. R. French, P. P. Niiler, T. B. Sanford, E. J. Terrill, E. J. Walsh, and J. Zhang, 2006: Air-sea exchanges in hurricanes: Synthesis of observations from the coupled boundary layer air-sea transfer experiment. *Bull. Amer. Meteor. Soc.*, accepted with revision.

Braun, S. A., 2002: A cloud-resolving simulation of hurricane Bob (1991): Storm structure and eyewall buoyancy. *Mon. Wea. Rev.*, **130**, 1573–1592.

-----, M. T. Montgomery, and Z. Pu, 2005: High-resolution simulation of Hurricane Bonnie (1998). Part I: The organization of eyewall vertical motion. *J. Atmos. Sci., NASA/CAMEX special issue*, **63**, 19 - 42.

Brown, O.B., and P.J. Minnett, 1999: MODIS infrared sea surface temperature algorithm theoretical basis document, ver 2.0, http://modis.gsfc.nasa.gov/data/atbd/atbd_mod25.pdf.

Camp, P. and M.T. Montgomery, 2001: Hurricane maximum intensity: Past and present. *Mon. Wea. Rev*., **129**, 1704 – 1717.

Cione, J., P. Black, and S. Houston, 2000: Surface observations in the hurricane environment. *Mon. Wea. Rev*. **128**, 1550 - 1561.

Cram, T. A., J. Persing, M. T. Montgomery, and S. A. Braun, 2005: A Lagrangian trajectory view on transport and mixing processes between the eye, eyewall and environment using a high resolution simulation of Hurricane Bonnie (1998). *J. Atmos. Sci.*, accepted.

Eastin, M.D., W.M. Gray, and P.G. Black, 2005: Buoyancy of convective vertical motions in the inner core of intense hurricanes. Part II: Case studies. *Mon. Wea. Rev*., **133**, 209 – 227.

Emanuel, K.A., 1986: An air-sea interaction theory for tropical cyclones. Part I: Steady-state maintenance. *J. Atmos. Sci*. **43**, 585 - 604.

-----, 1988: The maximum intensity of hurricanes. *J. Atmos. Sci.*, **45**, 1143 - 1155.

-----, 1991: The theory of hurricanes. *Annual Rev. Fluid Mech.,* **23**, 179-196.

-----, 1995: Sensitivity of tropical cyclones to surface exchange coefficients and a revised steady-state model incorporating eye dynamics. *J. Atmos. Sci*., **52**, 3969 – 3976.

-----, 1997: Some aspects of hurricane inner-core dynamics and energetics. *J. Atmos. Sci.*, **54**, 1014 - 1026.

-----, DesAutels, C., C. Holloway, and R. Korty, 2004: Environmental control of tropical cyclone intensity. *J. Atmos. Sci.* **61**, 843 - 858.

Flatau, M., and D.E. Stevens, 1989: Barotropic and inertial instabilities in the hurricane outflow layer. *Geophys. Astrophys. Fluid Dyn*., **47**, 1 – 18.

Hock, T.F. and J.L. Franklin, 1999: The NCAR GPS dropwindsonde. *Bull. Amer. Met. Soc.*, **80**, 407 - 420.

Holland, G., 1987: *Global View of Tropical Cyclones*, Section 2.7. R. Elsberry, Editor.

Holton, J. R., 2004: *An Introduction to Dynamic Meteorology*. Academic Press.

Houze, R., 1993: *Cloud Dynamics*. Academic Press.

Koch, S.E., M. Desjardins, and P.J. Kocin, 1983: An interactive Barnes objective map scheme for use with satellite and conventional data. *J. Climate Appl. Meteor.* **22**, 1487 – 1503.

Kossin, J.P., and W.H. Schubert, 2001: Mesovortices, polygonal flow patterns, and rapid pressure falls in hurricane-like vortices. *J. Atmos. Sci*. **58**, 2196 – 2201.

-----, and -----, 2004: Mesovortices in hurricane Isabel. *Bull Amer. Met. Soc.*, 151- 153.

LeeJoice, R. N., 2000: Hurricane inner-core structure as revealed by GPS dropwindsondes. Department of Atmospheric Science Bluebook No. 477, 56 pp.

Legeckis, R., and T. Zhu, 1997: Sea surface temperatures from the GOES-8 geostationary satellite. *Bull. Amer. Met. Soc.*, **78**, 1971 - 1983.

Montgomery, M.T., V. A. Vladimirov, and P.V. Denissenko, 2002: An experimental study on hurricane mesovortices. *J. Fluid. Mech.,* **471**, 1 – 32.

McMillin, L.M., and D.S. Crosby, 1984: Theory and validation of the multiple window sea surface temperature technique. *J. Geophys. Res.*, **89(C3)**, 3655 – 3661.

Moss, M.S., 1978: Low-layer features of two limited-area hurricane regimes. *NOAA Technical Report ERL 394-NHEML 1*, pp. 17-18.

Nolan, D. S., and M. T. Montgomery, 2002: Nonhydrostatic, three-dimensional perturbations to balanced, hurricane-like vortices. Part I: Linearized formulation, stability, and evolution. *J. Atmos. Sci.*, **59**, 2989–3020.

Persing, J., and M.T. Montgomery, 2003: Hurricane superintensity. *J. Atmos. Sci.* **60**, 2349 – 2371.

Rotunno, R., 1978: A note on the stability of a cylindrical vortex sheet. *J. Fluid Mech.*, **87**, 761-777.

-----, 1984: An investigation of a three-dimensional asymmetric vortex. *J. Atmos. Sci.*, **41**, 283 - 298.

-----, and K.A. Emanuel, 1987: An air-sea interaction theory for tropical cyclones. Part II: Evolutionary study using a nonhydrostatic axisymmmetric model. *J. Atmos. Sci.* **44**, 542 - 561.

Schubert, W.H., M.T. Montgomery, R.K. Taft, T.A. Guinn, S.R. Fulton, J.P. Kossin, and J.P. Edwards, 1999: Polygonal eyewalls, asymmetric eye contraction, and potential vorticity mixing in hurricanes. *J. Atmos. Sci.*, **56**, 1197 - 1223.

Shapiro, L. J., 1983: The asymmetric boundary layer flow under a translating hurricane. *J. Atmos. Sci.*, **40**, 1984 – 1998.

Smith, R. K., 1980: Topical cyclone eye dynamics. *J. Atmos. Sci.*, **37**, 1227 – 1232.

Sullivan, P., J. McWilliams, and W.K. Melville, 2004a: Impacts of breaking waves and Langmuir circulations on the ocean mixed layer in high winds. *Preprints, 26th Conf. on Hurricanes and Tropical Meteorology*, Amer. Meteor. Soc., Boston, MA, 54 - 55.

-----, ----- and ----- 2004b: The oceanic boundary layer driven by wave breaking with stochastic variability. I: Direct numerical simulations. *J. Fluid Mech.*, **507**, 143 - 174.

Vladimirov, V.A., V.I. Yudovich, M. Yu Zhukov, and P.V. Denissenko, 2001: Asymmetric flows induced by a rotating body in a thin layer. HIMSA Preprint, **3**, 45 pp.

Willoughby, H.E., 1990: Gradient balance in tropical cyclones**.** *J. Atmos. Sci.,* **47**, 265–274.

Wroe, D.R., and G.M. Barnes, 2003: Inflow layer energetics of Hurricane Bonnie (1998) near landfall. *Mon. Wea. Rev*. **131**, 1600 – 1612.

							Radial Outflow Layer			
Sounding	Radius from center (km)	RH (%)	T_B (°C)	T_O PM (°C)	T_O EL (°C)	T_O EMPI (°C)	θ_e Bottom (K)	Altitude Bottom (m)	θ_e Top (K)	Altitude Top (m)
G-IV 22:27:14 (NE)	341	72.6	24.9	-54.2	-59	-52.9	349.7	11140	358.8	14060
G-IV 20:04:13 (NW)	525	82.5	24.5	-43.4	-44	-54.4	349.7	11700	354.9	13210
G-IV 00:33:36 (SE)	347	77.7	23.8	-55.7	-50	-56.5	349.8	12090	359.2	14359
TJSJ 24:00:00 (SW)	584	84.2	24.3	-70.7	-78	-79.5	349.7	14109	359.2	16539
Average of 7 soundings	653.8	80.7	24.1	-52.9	-56.7	-57.8	349.7	12389	358.0	14801

Table 1. Observed and calculated environmental temperatures and RH for Hurricane Isabel on 13 September 2003**.** RH is the average in the lowest 500 m. Temperature at the boundary layer top (T_B), radial-wind-weighted outflow temperature (T_O PM), equilibrium-level outflow temperature (T_O EL), $d\ ln(\theta_e)$-weighted outflow temperature (T_O EMPI), and θ_e at the outflow layer top and bottom are also shown.

Figure Captions

Figure 1. Satellite and airborne radar imagery of Hurricane Isabel on 13 September. (a) SSMI 85 GHz brightness temperature at 2218Z (courtesy of NRL/Monterey); (b) Visible image at 1745 UTC from GOES super-rapid-scan operations; and (c) Radar reflectivity (in dBZ) from lower-fuselage (5 cm) radar onboard NOAA aircraft while flying inside the eye at ~2 km altitude. The time of the radar image (1747 UTC) is two minutes after the visible image shown in (b). In (a), (b) and (c) the horizontal scales of the images are approximately 1400 km, 300 km and 180 km, respectively. The mesovortices within the eye in (b) and the pentagonal shape of the high reflectivity in the eyewall in (c) are particularly striking features.

Figure 2. Dropwindsonde locations and trajectories and aircraft flight tracks relative to storm center from 16 – 23 UTC 13 September. Storm-relative data distribution in the (a) azimuthal (R-θ) plane; and (b) radial-height (R-Z) plane, showing the NOAA P-3 (42 in blue, 43 in green), USAF C-130 (in black) flight tracks, and dropwindsonde trajectories (in red). The dropwindsondes in (a) move cyclonically (counterclockwise).

Figure 3. Radius-height azimuthal mean structure derived from GPS dropwindsonde and flight-level data from 1600 – 2300 UTC 13 September. Top panel (a) shows storm-relative tangential wind (color) and radial wind (contour) in m s^{-1}. Bottom panel (b) shows θ_e (color, in Kelvin); absolute angular momentum (contour, $m^2 s^{-1} \times 10^6$); and transverse secondary circulation (vector). The origin (0, 0) denotes the eye center at the ocean surface.

Figure 4. Low-level (0 – 2 km) mean soundings from dropwindsonde observations for the eye

(0 – 15 km radius, red), nominal eyewall (40 – 50 km radius, orange), outer core (~200 km radius, green), and ambient environment (300 – 1000 km radius, blue) during 16 – 23 UTC 13 September. Panels are (a) tangential wind in m s^{-1}, (b) radial wind in m s^{-1} (inflow/outflow transition indicated by dashed line), (c) temperature in ˚C, (d) RH in percent, (e) θ_v in K, and (f) θ_e in K.

Figure 5. SST derived from AVHHR satellite (average from 4 to 10 September in color), ARGOS buoys, and NOAA P-3 downward-pointing radiometer (thin line, from 18 UTC 13 September). Tracks of Hurricanes Fabian (heavy dashed, from 2 to 5 September) and Isabel (thin dashed, with thick solid line indicating analysis period from 16 – 23 UTC on 13 September) are shown for reference.

Figure 6. (a) GOES infrared satellite imagery at 2215 UTC (courtesy of NRL/Monterey) showing extent of hurricane outflow, and the dropwindsonde profile locations (red dots with UTC time labels) used in the outflow temperature calculation. 'X' indicates location of additional outflow jet sample at 553 km radius from center, (b) High altitude wind speed (m s^{-1}) and θ_e (K) from NOAA Gulfstream-IV dropwindsonde at 341 km radius from center at 2227 UTC. Tangential (red) and radial (blue) winds show anticyclonic outflow, with θ_e in green. Black dashed line indicates linearly interpolated data.

Figure 7. Theoretically predicted azimuthal mean V_{max} at the boundary layer top assuming C_K/C_D =1 for varying outflow temperature and near-core SST with a constant RH = 80%. 'X' indicates the primary potential intensity estimate for the observed environment around Isabel (using a SST of 27.5 ˚C near the eyewall region associated with the Fabian wake), which yields a

56.6 m s^{-1} mean V_{max}. The dark solid curve represents the average storm-relative tangential wind speed at the top of the boundary layer derived from the dropwindsonde measurements, and the shading represents the 6 m s^{-1} standard deviation of this mean value. The vertical dashed line presents a range of mean intensities employing the same outflow temperature, SST, and RH used to obtain 'X' so as to reflect uncertainties in the bulk exchange ratio and the ocean cooling effect. The upper bound (~66 m s^{-1}) neglects entirely the ocean cooling, includes dissipative heating, and assumes that $C_K/C_D = 1$. The lower bound (~40 m s^{-1}) assumes $C_K/C_D = 0.5$, and assumes the ocean cooling effect is compensated by the dissipative heating effect. The discrepancy between these predicted values and the observed intensity suggests a significant limitation of E-MPI theory for this case.

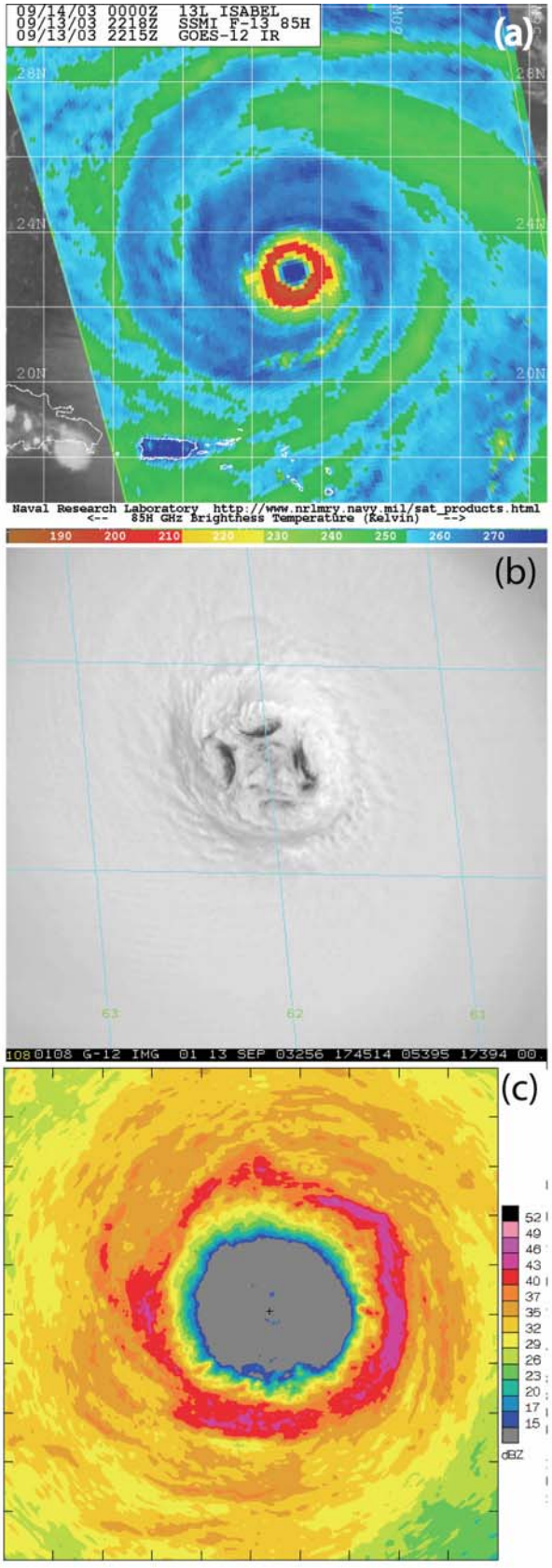
09/14/03 0000Z 13L ISABEL
09/13/03 2218Z SSMI F-13 85H
09/13/03 2215Z GOES-12 IR
(a)
28N
24N
20N
Naval Research Laboratory http://www.nrlmry.navy.mil/sat_products.html
<-- 85H GHz Brightness Temperature (Kelvin) -->
190 200 210 220 230 240 250 260 270
(b)
0108 0108 G-12 IMG 01 13 SEP 03256 174514 05395 17394 00
(c)
52
49
46
43
40
37
35
32
29
26
23
20
17
15
dBZ

Figure 1. Satellite and airborne radar imagery of Hurricane Isabel on 13 September. (a) SSMI 85 GHz brightness temperature at 2218Z(courtesy of NRL/Monterey) ; (b) Visible image at 1745 UTC from GOES super-rapid-scan operations; and (c) Radar reflectivity (in dBZ) from lower-fuselage (5 cm) radar onboard NOAA aircraft while flying inside the eye at ~2 km altitude. The time of the radar image (1747 UTC) is two minutes after the visible image shown in (b). In (a), (b) and (c) the horizontal scales of the images are approximately 1400 km, 300 km and 180 km, respectively. The mesovortices within the eye in (b) and the pentagonal shape of the high reflectivity in the eyewall in (c) are particularly striking features.

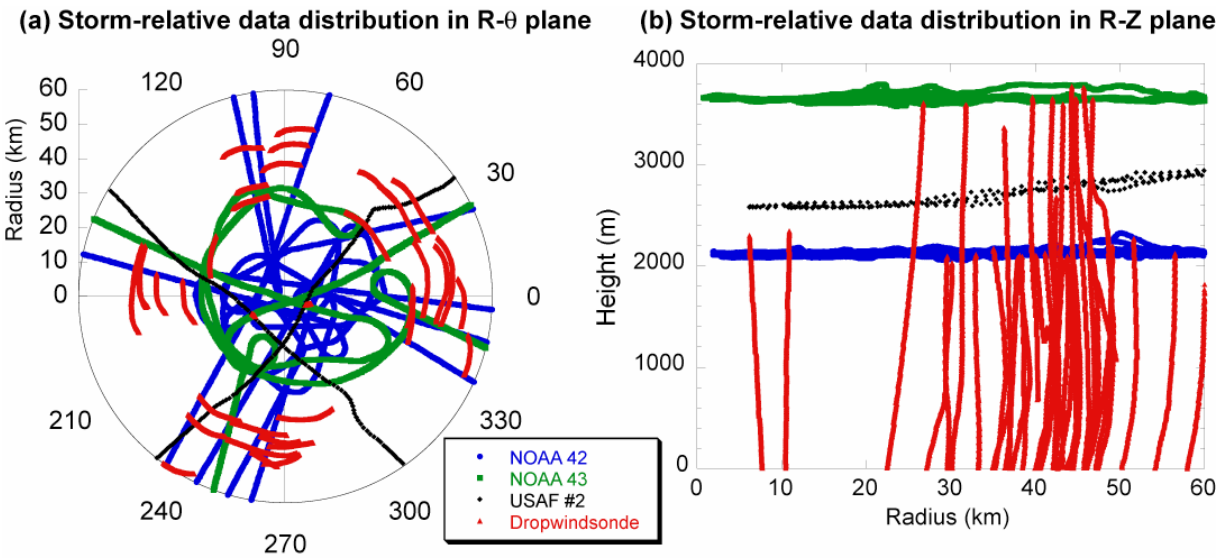

Figure 2. Dropwindsonde locations and trajectories and aircraft flight tracks relative to the storm center from 16 – 23 UTC 13 September. Storm-relative data distribution in the (a) azimuthal (R-θ) plane; and (b) radial-height (R-Z) plane, showing the NOAA P-3 (42 in blue, 43 in green), USAF C-130 (in black) flight tracks, and dropwindsonde trajectories (in red). The dropwindsondes in (a) move cyclonically (counterclockwise).

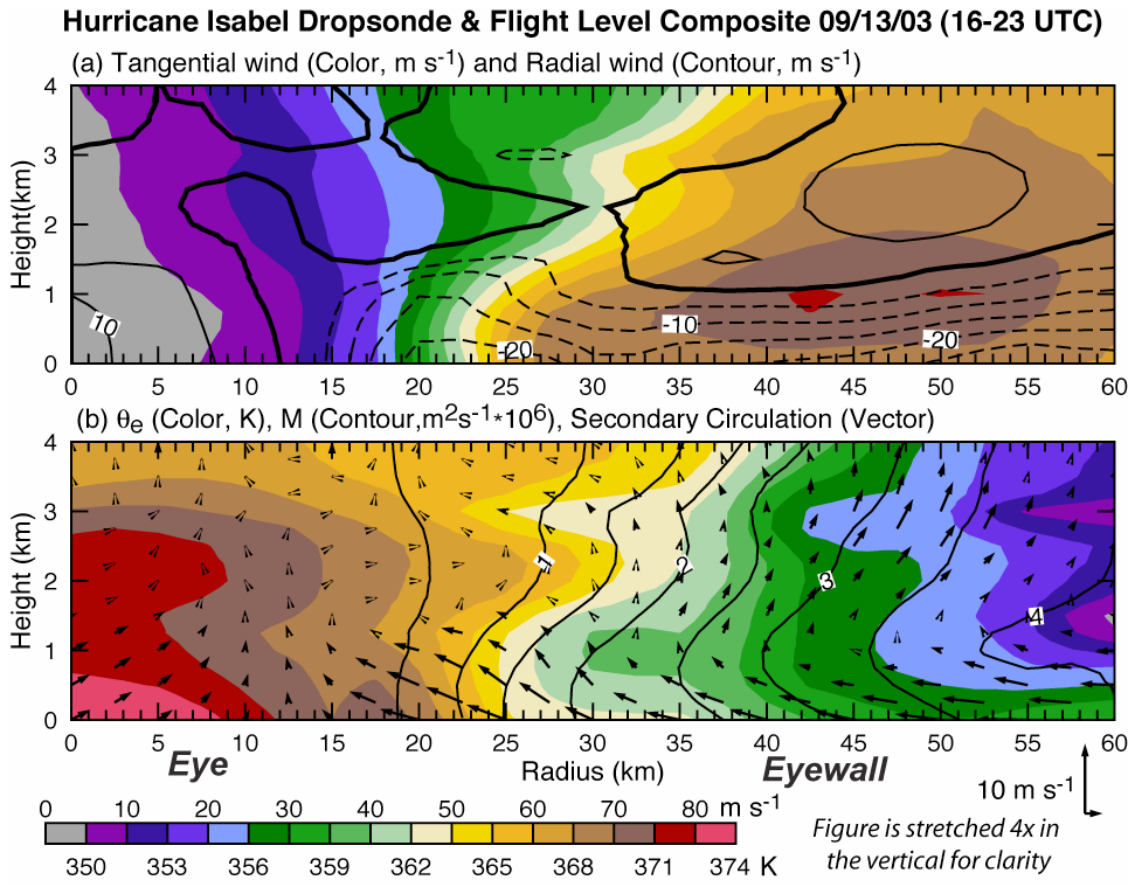

Figure 3. Radius-height azimuthal mean structure derived from GPS dropwindsonde and flight level data from 1600 – 2300 UTC 13 September. Top panel (a) shows storm-relative tangential wind (color) and radial wind (contour) in m s^{-1}. Bottom panel (b) shows θ_e (color, in Kelvin); absolute angular momentum (contour, $m^2\ s^{-1} \times 10^6$); and transverse secondary circulation (vector). The origin (0, 0) denotes the eye center at the ocean surface.

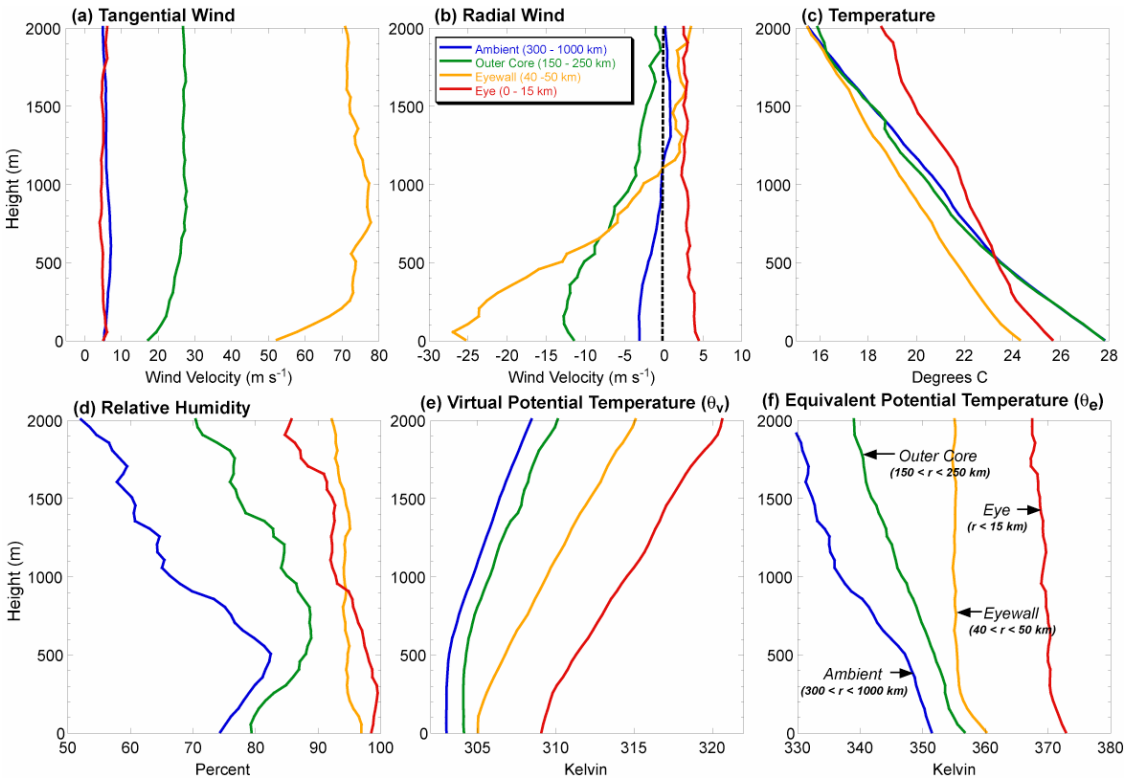

Figure 4. Low-level (0 – 2 km) mean soundings from dropwindsonde observations for the eye (0 – 15 km radius, red), nominal eyewall (40 – 50 km radius, orange), outer core (~200 km radius, green), and ambient environment (300 – 1000 km radius, blue) during 16 – 23 UTC, 13 September. Panels are (a) tangential wind in m s^{-1}, (b) radial wind in m s^{-1} (inflow/outflow transition indicated by dashed line), (c) temperature in ˚C, (d) RH in percent, (e) θ_v in K, and (f) θ_e in K.

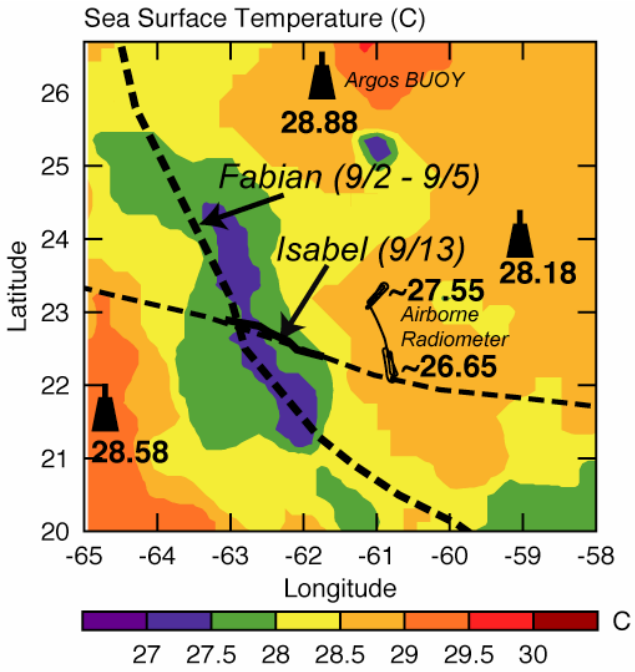

Figure 5. SST derived from AVHHR satellite (average from 4 to 10 September in color), ARGOS buoys, and NOAA P-3 downward-pointing radiometer (thin line, from 18 UTC 13 September). Tracks of Hurricanes Fabian (heavy dashed, from 2 to 5 September) and Isabel (thin dashed, with thick solid line indicating analysis period from 16 – 23 UTC on 13 September) are shown for reference.

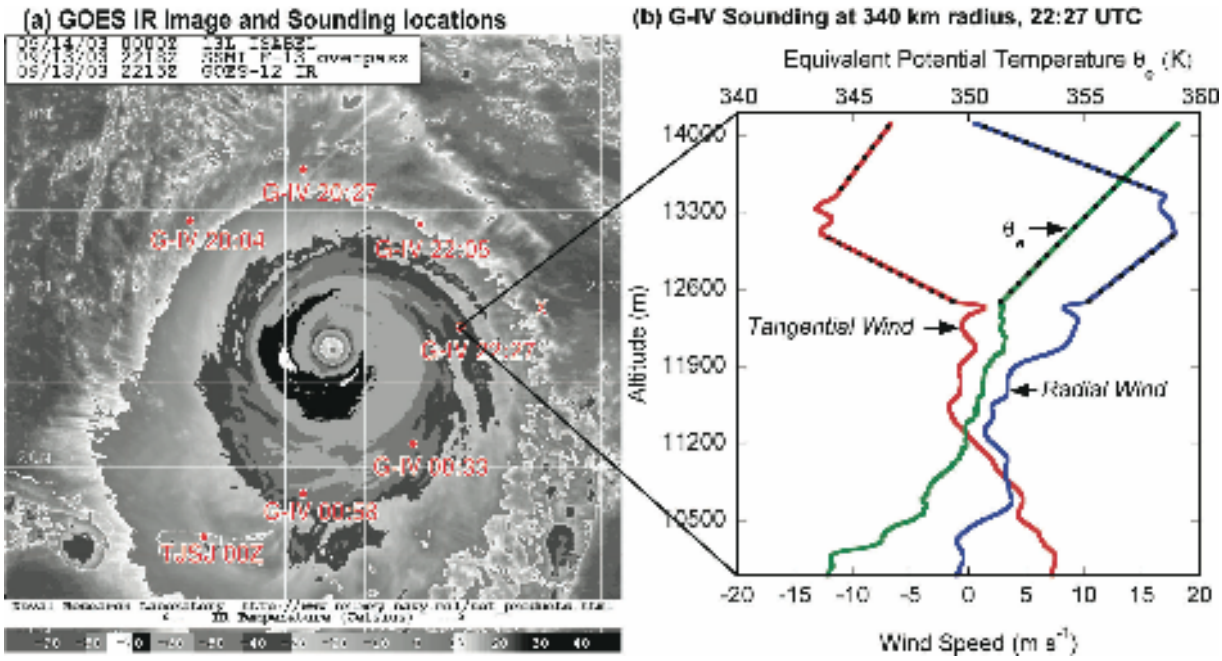

Figure 6. (a) GOES infrared satellite imagery at 2215 UTC (courtesy of NRL/Monterey) showing extent of hurricane outflow, and the dropwindsonde profile locations (red dots with UTC time labels) used in the outflow temperature calculation. 'X' indicates location of additional outflow jet sample at 553 km radius from center, (b) High altitude wind speed (m s^{-1}) and θ_e (K) from NOAA Gulfstream-IV dropwindsonde at 341 km radius from center at 2227 UTC. Tangential (red) and radial (blue) winds show anticyclonic outflow, with θ_e in green. Black dashed line indicates linearly interpolated data.

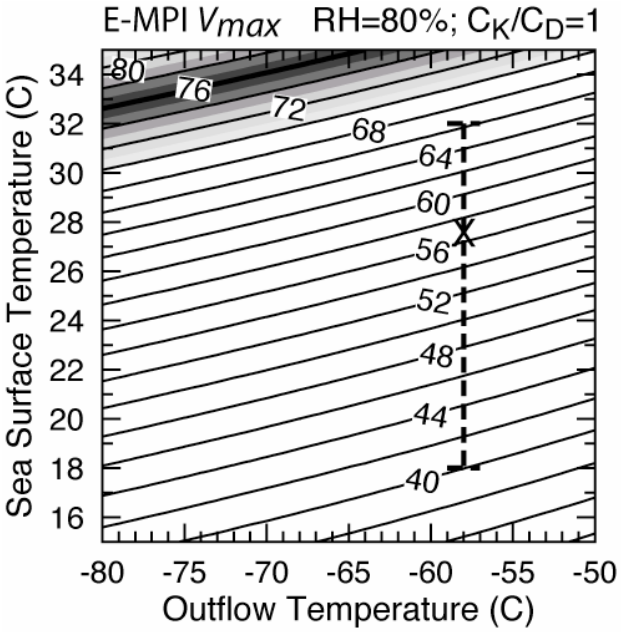

Figure 7. Theoretically predicted azimuthal mean V_{max} at the boundary layer top assuming C_K/C_D =1 for varying outflow temperature and near-core SST with a constant RH = 80%. 'X' indicates the primary potential intensity estimate for the observed environment around Isabel (using a SST of 27.5 ˚C near the eyewall region associated with the Fabian wake), which yield a 56.6 m s^{-1} mean V_{max}. The dark solid curve represents the average storm-relative tangential wind speed at the top of the boundary layer derived from the dropwindsonde measurements, and the shading represents the 6 m s^{-1} standard deviation of this mean value. The vertical dashed line presents a range of mean intensities employing the same outflow temperature, SST, and RH used to obtain 'X' so as to reflect uncertainties in the bulk exchange ratio and the ocean cooling effect. The upper bound (~66 m s^{-1}) neglects entirely the ocean cooling, includes dissipative heating, and assumes that C_K/C_D = 1. The lower bound (~40 m s^{-1}) assumes C_K/C_D = 0.5, and assumes the ocean cooling effect is compensated by the dissipative heating effect. The discrepancy between these predicted values and the observed intensity suggests a significant limitation of E-MPI theory in this case.